Promega

Don’t settle for just a supplier. Find a custom manufacturing partner.

Your specifications. Your format.

Our scientists waiting to help.

Let’s TALK CUSTOM

40+ years CUSTOM EXPERIENCE

5 GLOBAL Mfg Sites

PRIMARY MANUFACTURER

Selecting a supplier for your biotechnology and biopharma products can be a challenge—especially one who can adapt to your specific needs. Don’t settle for just a supplier. Instead, partner with Promega and work with a custom manufacturer willing to provide you with the scientific expertise, ongoing technical support and quality standards that support your success.

Learn more with our video:
promega.com/CustomProcess

ARTICLE

BIOTECHNOLOGY and BIOENGINEERING

Oxygen Mapping: Probing a Novel Seeding Strategy for Bone Tissue Engineering

Ines Westphal,[1,2] Claudia Jedelhauser,[1] Gregor Liebsch,[3] Arnd Wilhelmi,[4] Attila Aszodi,[1] Matthias Schieker[1,2]

[1]Experimental Surgery and Regenerative Medicine, Department of General, Trauma and Reconstruction Surgery, University Hospital, Ludwig-Maximillians-University of Munich, Nussbaumstr. 20, Munich 80336, Germany; telephone: +49-(0)89 4400 55470; fax: +49-(0)89 4400 55482; e-mail: ines.westphal@med.uni-muenchen.de; e-mail: matthias.schieker@med.uni-muenchen.de

[2]LivImplant GmbH, Starnberg, Germany

[3]PreSens Precision Sensing GmbH, Regensburg, Germany

[4]Tutogen Medical GmbH, Neunkirchen am Brand, Germany

ABSTRACT: Bone tissue engineering (BTE) utilizing biomaterial scaffolds and human mesenchymal stem cells (hMSCs) is a promising approach for the treatment of bone defects. The quality of engineered tissue is crucially affected by numerous parameters including cell density and the oxygen supply. In this study, a novel oxygen-imaging sensor was introduced to monitor the oxygen distribution in three dimensional (3D) scaffolds in order to analyze a new cell-seeding strategy. Immortalized hMSCs, pre-cultured in a monolayer for 30–40% or 70–80% confluence, were used to seed demineralized bone matrix (DBM) scaffolds. Real-time measurements of oxygen consumption in vitro were simultaneously performed by the novel planar sensor and a conventional needle-type sensor over 24 h. Recorded oxygen maps of the novel planar sensor revealed that scaffolds, seeded with hMSCs harvested at lower densities (30–40% confluence), exhibited rapid exponential oxygen consumption profile. In contrast, harvesting cells at higher densities (70–80% confluence) resulted in a very slow, almost linear, oxygen decrease due to gradual achieving the stationary growth phase. In conclusion, it could be shown that not only the seeding density on a scaffold, but also the cell density at the time point of harvest is of major importance for BTE. The new cell seeding strategy of harvested MSCs at low density during its log phase could be a useful strategy for an early in vivo implantation of cell-seeded scaffolds after a shorter in vitro culture period. Furthermore, the novel oxygen imaging sensor enables a continuous, two-dimensional, quick and convenient to handle oxygen mapping for the development and optimization of tissue engineered scaffolds.

Biotechnol. Bioeng. 2017;114: 894–902.

KEYWORDS: bone tissue engineering; mesenchymal stem cells; 3D scaffolds; oxygen measurement; time point of harvest; cell density

Conflict of interest: I.W., C.J., A.A. and M.S. declare that no competing financial interests exist for this project. G.L. is employee and head of R&D imaging solutions of PreSens-Precision Sensing GmbH and A.W. is employee and director of pharmacovigilance of Tutogen Medical GmbH.

Correspondence to: I. Westphal and M. Schieker

Contract grant sponsor: Bayerische Forschungsstiftung

Received 29 April 2016; Revision received 12 September 2016; Accepted 14 October 2016

Accepted manuscript online 14 October 2016;

Article first published online 17 November 2016 in Wiley Online Library (http://onlinelibrary.wiley.com/doi/10.1002/bit.26202/abstract).

DOI 10.1002/bit.26202

Introduction

Optimal treatment of bone fractures and bone diseases is of pivotal importance in clinical-experimental research (Ceccarelli et al., 2013). To date, bone replacement grafts are seen as the gold standard and have an established role in the treatment of various bone diseases like tumor resections, traumatic bone loss, hereditary bone diseases, and osteoporotic fractures (Dimitriou et al., 2011; Elsalanty and Genecov, 2009; Fayaz et al., 2011; Korompilias et al., 2011; Oryan et al., 2014; Pederson and Person, 2007). The latter are most alarming since they cause severe clinical problems due to their high frequency of occurrence (Hernlund et al., 2013). However, the use of bone replacement grafts is limited due to the availability of suitable donor material and the high incidence of donor-site-morbidity (Ahlmann et al., 2002; Dimitriou et al., 2011). A promising alternative is the in vitro engineering of bone graft substitutes (Dimitriou et al., 2011). Cells with osteogenic potential, as for example hMSC, are cultivated in three-dimensional scaffolds, mimicking a basic bone environment for cell adhesion, migration, proliferation, and differentiation, prior to their therapeutic application (Ceccarelli et al., 2013).

However, the clinical application of engineered bone tissue is still in its early days and rather limited. One of the major concerns hindering development for wide-spread use, is a missing standard

for culturing and harvesting hMSC before transplantation (Colter et al., 2000; Kim et al., 2014; Neuhuber et al., 2008; Polzer et al., 2014). Different culture conditions, such as varying densities of cells, can affect the quality of the engineered graft and influence growth kinetics and furthermore gene expression pattern (Colter et al., 2000; Neuhuber et al., 2008). Therefore, it is necessary to investigate and determine the optimal conditions for culturing and harvesting (Kim et al., 2014). Furthermore, it is well-known that variation in oxygen levels throughout the 3D scaffold significantly influences tissue formation (Malladi et al., 2006; Radisic et al., 2006; Volkmer et al., 2008). Scaffolds, longer than 5 mm in size, show steep oxygen gradients ranging from almost hypoxic centers to adequate oxygen levels at peripheral regions (Volkmer et al., 2008, 2010, 2012). This in turn results not only in a heterogeneous cell distribution, oxidative stress, and metabolic reprogramming of the engineered tissue but furthermore in a reduced or completely disappeared osteogenic potential at the inner region of the scaffold (Benjamin et al., 2013; Malladi et al., 2006). To circumvent such a characteristic outcome, one has to constantly monitor the oxygen levels and supply oxygen if required (Volkmer et al., 2008; Yeatts et al., 2013). There are several methods available for oxygen measuring, which are either based on microsensors or microplates (Janssen et al., 2010; Volkmer et al., 2008). Microsensors are invasive and probe the oxygen concentration only locally (e.g., needle type sensors), while microplates only probe the oxygen concentration of the surrounding environment.

To monitor 2D or even 3D of oxygen level variations within a scaffold, a novel, planar oxygen imaging device offers the possibility to not only visualize oxygen distribution across a whole scaffold but also monitor oxygen changes over time (Tschiersch et al., 2011, 2012). To date, this novel method is applied in several different fields, including neurosurgery, plastic surgery, and physiological research (Hofmann et al., 2013; Meier et al., 2012; Ochs et al., 2014; Woertgen et al., 2009). In this study, we have adapted and utilized the novel oxygen imaging method to investigate oxygen distribution in cell-seeded 3D scaffolds allowing the characterization of modified cell-seeding strategies for BTE. In this context, we analyzed the oxygen consumption of DBM scaffold cultures seeded with cells from different confluences at the point of harvest.

Materials and Methods

Cell Culture

Immortalized human mesenchymal stem cell line hMSC-SCP-1 (Bocker et al., 2008) were cultured in nutrition medium consisting of alpha minimal essential medium (αMEM; Invitrogen, Carlsbad, CA) supplemented with 10% fetal bovine serum (FBS; Sigma–Aldrich, St. Louis, MO) and 40 IU/mL penicillin/streptomycin (PAA Laboratories GmbH, Pasching, Austria). Cells were incubated in a humidified atmosphere of 95% air and 5% carbon dioxide (CO_2) at 37 °C. The medium was changed twice a week. For the experiments, MSCs were plated in cell culture flasks (Nunc-Thermo Fisher Scientific, Waltham, MA) at a density of 6.7×10^3 cells/cm^2 (equal to 5×10^5 cells per T75 flask) to achieve a final 70–80% confluence and 2.2×10^3 cells/cm^2 (equal to 5×10^5 cells per T225 flask) to get a final 30–40% confluence at the time of harvest. Cells were cultured for about 2 days until they reached target confluence.

3D Scaffold Culture

Demineralized bone matrix (DBM; Tutogen, Neunkirchen, Germany) with 5 mm height and 9 mm diameter was used as 3D constructs. Before cell seeding, DBM scaffolds were centrifuged at 500*g* in nutrition medium to remove air bubbles within the scaffolds. This procedure was repeated several times until the medium did not change its color indicating a constant pH-value.

The DBM scaffold was seeded statically with hMSC-SCP-1 cells harvested either at low confluence (30–40%, population L), or at high confluence (70–80%, population H). Cells were washed twice with phosphate buffered saline (PBS), trypsinized with 1× Trypsin/EDTA (PAA Laboratories GmbH), neutralized with nutrition medium and centrifuged at 500*g* for 5 min. The pellets were resuspended with a concentration of either 5×10^5 or 1×10^6 cells per 500 μL of αMEM and pipetted on the top of the DBM scaffold situated in a 48-well dish (Nunc-Thermo Scientific). After 10 min, scaffolds were turned three times and twice after 15 min of incubation at 37 °C, and the flow out cell suspension was re-pipetted onto the scaffold at each time. Thereafter, the cell-seeded constructs were transferred into 24-well plates and cultured with 1 mL nutrition media per well for 24 h at 95% air and 5% CO_2 at 37 °C.

Oxygen Imaging Sensor

The novel oxygen imaging device (VisiSens; PreSens, Regensburg, Germany) consists of a compact fluorescence microscope detector unit (DU 01) and an optical sensor foil (SF-RPSu4). The system is based on a fluorescence quenching technique. The optical sensor foil includes a reference dye and an indicator dye, which is sensitive to oxygen. Interactions of oxygen molecules with the indicator dye are causing quenching of the fluorescence signal. Consequently, the fluorescence signal of the indicator dye decreases when oxygen in the probe increases. The reference dye remains unaffected. For the oxygen measurement, both dyes were excited by a blue LED light source. Their emission spectra differ, the indicator dye emits in the red and the reference dye in the green spectrum. Both signals are captured within a single RGB image and relevant oxygen concentrations are computed from the ratio between the red and green channels (considering a calibration function derived from exposure of the sensor to a known oxygen concentration). The foils are flexible and based on a transparent polyester support, thus they can be cut to any desired size to fit the experimental requirements. A non-transparent optical isolation layer above prevents cross-talk by optical interferences, such as sample auto-fluorescence or ambient light. If optical interferences can be largely excluded, the isolation layer may be peeled off, resulting in completely functional and semi-transparent sensor foils. The sensor acts as a simultaneous interpreter, translating concentrations of oxygen into specific light signals. Each dye molecule inside the sensor foil reacts independently and the light signals can be recorded with the digital camera inside the detector unit. One single image contains the information of a whole array of single sensor points. This way the oxygen distribution over a large 2D area can be visualized and

subsequently analyzed with a high spatial resolution (μm-scale). The resulting data are transferred via a USB-connection to the processing unit and oxygen levels can be directly displaced and analyzed by the software VisiSens AnalytiCal 1 (PreSens). More technical specifications can be found elsewhere (Tschiersch et al., 2011, 2012).

Oxygen measurements were carried out hourly over a period of 24 h.

Application of the Oxygen Imaging Sensor for Bone TE

In order to adapt the novel oxygen imaging system for BTE purposes, the following experimental setup was established in a 48-well culture dish (Fig. 1A and B). The optical sensor foil was adjusted to the shape of the wells and the isolation layer was removed over the sensitive layer to avoid air bubbles between the layers. To prevent microbial infections, the sensor foil was sterilized in 80% ethanol for 20 min, rinsed in sterile PBS and placed at the bottom of a well. A cell-seeded DBM scaffold was laid on the top of the foil, covered with fresh medium avoiding the formation of air bubbles. The culture dish was then transferred into a humidified CO_2 incubator. The detector unit was installed inside the incubator directly under the monitored well. To achieve a close contact between the sensor foil and the detector unit, a small window was prepared into the upper incubator shelf. As a control for the novel oxygen imaging system, a needle-type sensor was also inserted into the center of the DBM scaffold for simultaneous oxygen measurement by a standardized method described previously (Volkmer et al., 2008, 2012). For the required two-point calibration, an unseeded DBM scaffold in fresh medium was used as 100% (equals 21% pO2) oxygen reference point. The 0% oxygen reference was performed by an unseeded scaffold, moistened with sodium sulphite (Na_2SO_3) which consumes oxygen by forming sodium sulphate (Na_2SO_4). Calibration values were recorded by evaluating a region of interest (ROI) as polygon over the lower scaffold surface. Areas outside the scaffold were not included for calibration. For valid investigations, newly engaged sensor foils or modification in the experimental design required a new calibration due to changes in background signals. The evaluation of oxygen consumption was performed by the VisiSens software AnalytiCal 1.

The novel sensor enables oxygen mapping by a color-coded graphical representation (Fig. 1D). In the resulting images, oxygen saturation is shown with a color spectrum. High oxygen levels are displayed with bright color, for example 21% oxygen saturation is shown in yellow. In contrast, low oxygen levels are represented with dark colors, for example, 0% oxygen saturation corresponds to a deep blue signal (Fig. 1D). Line-scans were additionally generated to plot a profile of the oxygen distribution across the equator of the imaged area (Fig. 1E). The typical oxygen map of a cell-seeded DBM scaffold after 24 h of culturing exhibits a clear oxygen gradient at the lower surface. The color transition from yellow–red to blue reveals decreasing oxygen tension from peripheral to central areas of the scaffold (Fig. 1D).

Needle-Type Oxygen Sensor

The oxygen measurement by a needle-type sensor (NFSx-PSt1; PreSens) has been described previously (Volkmer et al., 2008, 2012) and it offers a suitable control to validate the measurement of the novel oxygen imaging sensor. Briefly, the optical microsensors were mounted on the 50 μm tip of optical fibers and inserted within a 0.4 mm hollow needle for protection. Before application, a two-point calibration was performed: 100% CO_2 as 0% oxygen reference and ambient air as 21% oxygen reference. To record oxygen pressure, the needle sensor was introduced into the geometric center of the scaffold.

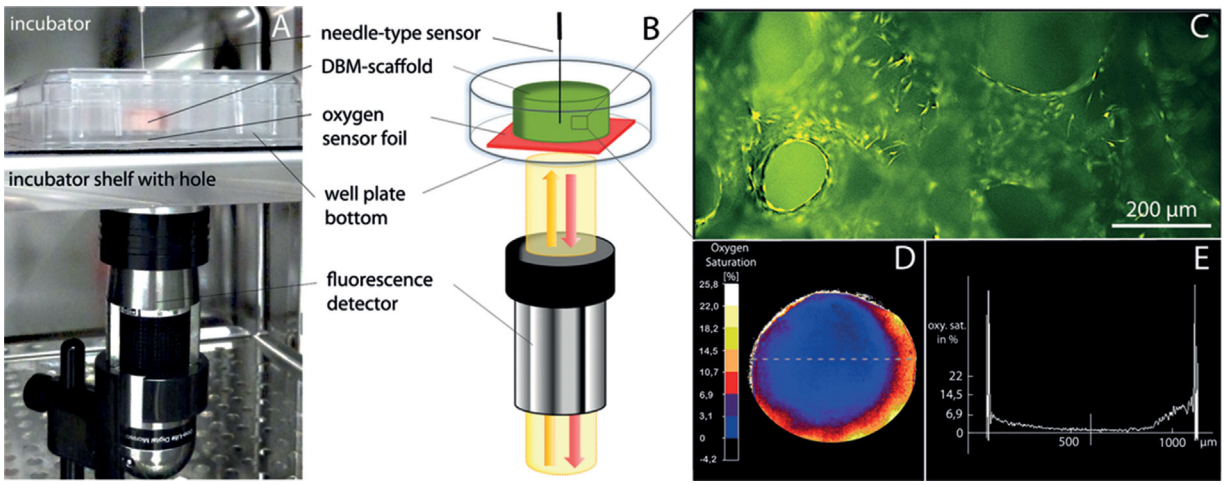

Figure 1. Experimental set-up of oxygen mapping. Original set-up is shown in (**A**) and as schematic representation in (**B**). The chemical sensor foil for oxygen detection was placed under the scaffold, whereas the portable fluorescence detector was installed directly underneath the well. To compare and validate the novel oxygen sensor, a well-established needle-type sensor was injected inside the scaffold centre. (**C**) Fluorescence image of a cell-seeded scaffold. Living cells were stained with calcein AM (green). (**D**) Exemplary image of a typical color-coded 2D-oxygen map generated by the oxygen-imaging sensor. (**E**) Line-scan deduced from the oxygen map (D, dashed line) shows the oxygen distribution across the center.

Live-Dead Assay

Cell survival in the scaffold was assessed by the Live/Dead® cell staining kit (Invitrogen), utilizing Calcein AM (green) to stain living cells and Ethidiumbromid-III (red) to detect dead cells. DBM scaffolds, cultivated for 24 h, were stained, cut into halves and living/dead cells were monitored by fluorescent microscopy using an Axio Observer Z1 microscope (Carl Zeiss Microscopy GmbH, Jena, Germany). Images were aquired with a Plan Neofluar 1,25× objective and a AxioCam MRm camera and processed using Zeiss AxioVision software.

Cell Metabolic and Proliferation Assay

Cell metabolic activity in the scaffold was assessed by the WST-1® colorimetric assay (Roche, Mannheim, Germany) measuring the cellular mitochondrial dehydrogenase activity-dependent cleavage of tetrazolium salt WST-1 into formazan. After 1, 6, 24, and 48 h of cultivation, WST-1 assay was performed by adding the cell proliferating reagent and measuring the optical density (OD) of the samples at 450 and 620 nm with a microplate photometer (Multiskan FC Microplate, Thermo Fisher Scientific). The initial cell proliferation potential of population L and H was measured by the CyQuant® cell proliferation assay (Thermo Fisher Scientific). 1×10^5 cells were seeded in microwell plates and the fluorescence emission of the total DNA was analyzed at 520 nm with a multiwell plate reader (Tecan Systems, Inc., San Jose, CA).

Statistical Analysis

Each experiment was repeated at least three times. The resulting data of the 2D oxygen sensor was analyzed by the appropriate software VisiSens AnalytiCal 1. Curve fittings and graphs were realized by Excel (Microsoft, Redmond). Statistical analysis was performed by Student's t-test ($P < 0.05$) using Sigma Plot version 12.0 (Systat Software, Erkrath, Germany). Data are presented as arithmetic mean and error bars of standard deviation (± SD).

Results

Comparison of Oxygen Mapping of DBM Scaffolds Seeded With Cells From Distinct Confluent Populations

The novel oxygen sensor was applied to characterize oxygen consumption in order to analyze novel cell-seeding strategies in DBM scaffolds. For this purpose, the scaffolds were seeded with different numbers of hMSC-SCP-1 cells (1×10^6 and 5×10^5), which were previously cultured in monolayer to either 70–80% (population H) or 30–40 % (population L) confluency (Fig. 2A and B). The oxygen consumption was recorded every hour over a period of 24 h. The comparison of the ROI of the oxygen maps revealed a clear difference in the timely progression of the oxygen consumption between populations H and L. Both the color coded images and the line scans demonstrated a faster and more homogenous oxygen depletion in scaffolds seeded with population L hMSCs (Fig. 2E, H, and I) compared to scaffolds seeded with population H cells (Fig. 2C, F, and G).

Using 1×10^6 cells of population L, the oxygen saturation curve showed a fast exponential-like drop already after 9 h ($R^2 = 0.97$) and reached 0% (± 0.5 SD) after 10 h (Fig. 2E and 3B blue line). In contrast, oxygen consumption of population H revealed a continuously slow, nearly linear decrease until 7.5% (± 4.6 SD, $R^2 = 0.94$) without touching the 0% oxygen level even after 24 h (Fig. 2C and 3A blue line). Student's t-test resulted in a statistically significant difference between oxygen consumption of population L and H from 1 until 24 h of incubation ($P < 0.01$ at 5–15 h, $P < 0.05$ for the remaining time).

A similar trend was observed in scaffolds seeded with 5×10^5 cells (Fig. 3C and D blue line), although the oxygen consumption proceeded slower compared with 1×10^6 cells. Using population H, the oxygen consumption curve exhibited a nearly linear decrease of not more than 5.6% (mean saturation 13.4% ± 0.6 SD, $R^2 = 0.97$) after 24 h (Fig. 3C blue line). In the case of population L, oxygen concentration reached 0% (± 0.7 SD) only after 16 h of incubation by an exponential drop (Fig. 3D blue line, $R^2 = 0.99$). The differences between oxygen consumption of population H and L of 5×10^5 cells were statistically highly significant from 5 h to 24 h of cultivation ($P < 0.01$) and significant between 2 and 5 h ($P < 0.05$).

In summary, oxygen saturation in scaffolds seeded with population H linearly dropped from 19% to 20% to 7.5% (± 4.6 SD) using 1×10^6 cells and to 13.4% (± 0.6 SD) with 5×10^5 cells after 24 h of incubation. In contrast, oxygen saturation of population L reached already 0% after 10 h (± 0.5 SD) for 1×10^6 and after 16 h (± 0.7 SD) for 5×10^5 cells. Oxygen saturations of population L decreased by a relatively clear exponential decay.

Comparison of Novel Oxygen Imaging Sensor and Needle-type Control Sensor in the Application of BTE

To validate the novel, non-invasive oxygen-imaging sensor for application in BTE, oxygen consumption in the scaffolds was measured simultaneously with an established needle-type sensor as control (15, 17). The comparison of these two sensors revealed similar characteristics of the oxygen consumption curves (Fig. 3).

The measurement of the control sensor started with an oxygen concentration of about 19–20% (Fig. 3A–D red line). After 24 h, the needle-type sensor showed a slow decrease of oxygen tension to 10.4% (± 1.9 SD) in scaffolds seeded with 1×10^6 cells of population H (Fig. 3A red line). Oxygen saturation quickly dropped to 1.5% (± 1.4 SD) when 1×10^6 cells were used from population L (Fig. 3B red line). In scaffolds seeded with 5×10^5 cells, oxygen concentrations approached 16.2% (± 0.8 SD) using population H (Fig. 3C red line) and 7.2% (± 2.4 SD) using population L (Fig. 3D red line) after 24 h of incubation time.

Oxygen measurement of four independent cell-seeded scaffolds per group (four groups in total) showed comparable oxygen graphs with an overall difference of 3.3% (± 2.6 SD) between values recorded by the oxygen imaging sensor and the needle-type sensor (Fig. 3). For each experiment the difference was analyzed at every time point. The difference between the two sensor types can be explained by their different measurement principles (point vs. area)

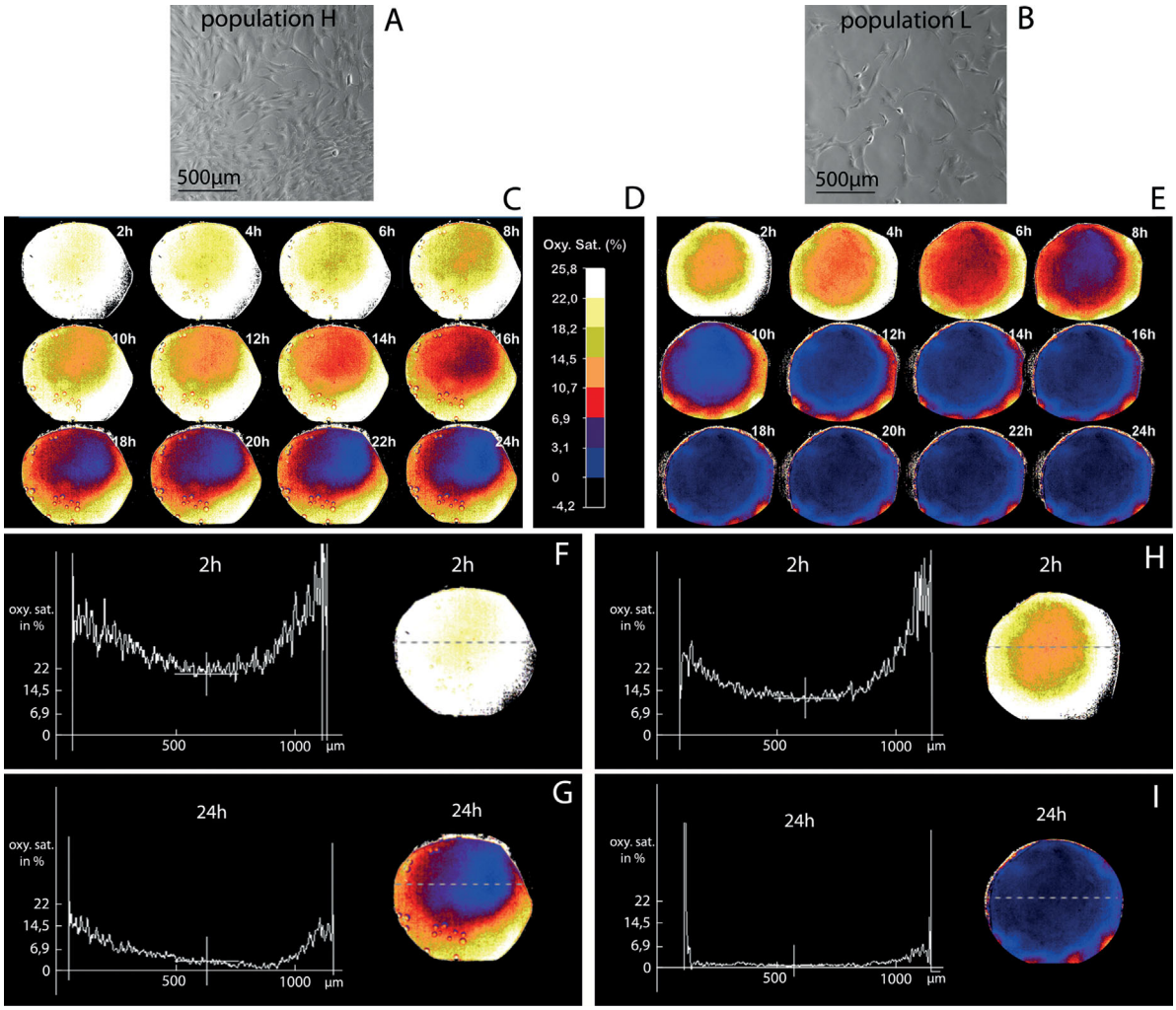

Figure 2. 2D-oxygen mapping by the novel oxygen-imaging sensor. (**A** and **B**) Phase contrast micrographs of population H and L at the time point of harvest. (**C** and **E**) Oxygen maps of scaffolds seeded with 1×10^6 cells of population H and L over 24 h. (**D**) Colour coded oxygen scale in percentage [%]. (F-I) Line scans from oxygen maps taken across the centre of the scaffold area (dashed line) at time point 2 h and after 24 h (n = 3).

and their respective locations within the scaffold (inside vs. outside). Figure 3D shows the largest difference between the two sensors. The needle sensor measured a lower oxygen consumption over 24 h, whereas the planar sensor detected a higher oxygen consumption. A reason for this result is the high growth and metabolic activity of population L and the much lower number of cells (1×10^5 cells) used in this experiment. During the seeding procedure more cells attach to the outer surfaces of the scaffold, resulting in a higher oxygen consumption which is measured by the planar oxygen sensor. In contrast, the lower number of cells inside the scaffold leads to a reduced oxygen consumption detected by the needle sensor.

Cell Metabolic Activity and Initial Proliferation

For an evaluation of cell survival and performance in scaffolds seeded with 5×10^5 and 1×10^6 cells of population L and H, a metabolic activity assay (WST) was applied (Fig. 4A and B). The WST assay shows increasing metabolic activity over 24 h for both populations, but decreasing activity between 24 and 48 h for population L (Fig. 4A and B). In contrast, metabolic activity of population H rises constantly. The increase of metabolically active cells differs clearly between the population L and H as well as between the cell densities of 1×10^6 and 5×10^5 cells. Most notable is the large difference between population L and H. Population L starts with an approximately 30% higher metabolic activity (1×10^6 cells, 0.65 OD ± 0.05 SD; 5×10^5 cells, 0.37 OD ± 0.01 SD) than population H (1×10^6 cells, 0.46 OD ± 0.062 SD; 5×10^5 cells, 0.26 OD ± 0.007 SD), even though both populations started always with the same cell numbers (1×10^6 or 5×10^5).

To show the initial difference in the proliferation activity of populations L and H, we analyzed their DNA content in a planar micro-well plate seeded with 1×10^5 cells. The fluorescence signal (FL) of the CyQuant assay revealed that population L starts with an around 50% higher DNA content (4,000 FL ± 258 SD) than population H (2,018 FL ± 37 SD) (Fig. 4C).

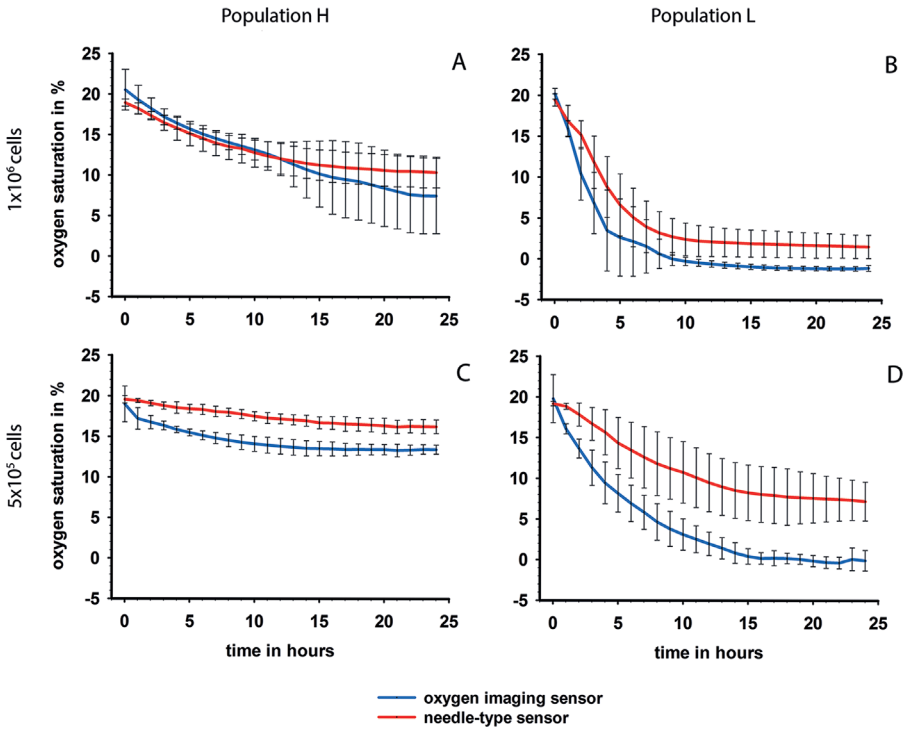

Figure 3. Graphical representation of average oxygen consumption over 24 h. (**A**–**D**) Oxygen consumption of scaffolds seeded with either 1×10^6 or 5×10^5 cells from population H and population L. Diagrams illustrate oxygen tension curves recorded by the foil-type imaging sensor (blue line) and the needle-type sensor (red line). A statistical difference of oxygen consumption ($P < 0.01$) was detected using the imaging sensor between population H and L from 5 to 15 h (**A** and **B**, 1×10^6 cells) and from 5 to 24 h (**C** and **D**, 5×10^5 cells). Regression analyses of the graphs show an almost, or precise, exponential drop in population L (1×10^6 cells $R^2 = 0.97$; 5×10^5 cells $R^2 = 0.99$) and in population H (1×10^6 cells $R^2 = 0.94$; 5×10^5 cells $R^2 = 0.97$). Values are measured by a region of interest (ROI). The area of the scaffold was outlined and the mean of the colour intensity was calculated. *P*-values were calculated with Student's t-test ($n = 3 \pm SD$).

To assess cell vitality across the scaffold, we used a live/dead fluorescence staining assay. Figure 4D and E shows viable cells (green) distributed all over the scaffold for the fastest growing population L with 1×10^6 cells. It must be noted that the DBM scaffold contains dead osteocytes which contribute to an unwanted background signal when performing the live/dead assay. It is therefore important to obtain a reference image of a cell-free DBM scaffold, which can be subtracted from the seeded scaffold.

Discussion

A Planar Oxygen Imaging Sensor for Oxygen Mapping of BTE Constructs

In this study, we have applied a novel 2D oxygen-imaging sensor to characterize modified cell-seeding strategies by quantifying the oxygen concentration in loaded DBM-scaffolds.

In the first step, we have adapted the novel sensor for BTE. Compared with a conventional needle-type sensor measuring oxygen in a single spot, the imaging sensor provides 2D-representation of oxygen concentration over a planar surface area, at a microscopic resolution (Tschiersch et al., 2012; Volkmer et al., 2008). This method has the advantages of being non-invasive and highly sensitive, whereas the injected needle-type sensor may induce injuries of the tissue or TE construct and generates unwanted gradients of material quality. The oxygen imaging sensor system is accompanied by user-friendly visualization and online analysis tools. Oxygen saturation can be displayed in conventional or color-coded diagrams and as line-scans (Fig. 2). The application of the oxygen imaging sensor is a very convenient and economical solution. The equipment, consisting of a sensor foil and a detector unit, is reusable, compact, and space-saving. The sensor tolerates a temperature-range from 5 to 45 °C, enabling a comfortable installation in a standard cell culture incubator. Details on the application of the novel sensor for BTE are described above (see results and Fig. 1).

We have previously reported that a conventional, needle-type sensor reliably measures oxygen concentration in static and dynamic 3D culture systems over a period of time (Volkmer et al., 2008, 2012). In the present study, in order to validate the oxygen values obtained by the novel planar sensor, the data were compared to values recorded by the needle system. In four independent experiments using scaffolds seeded with different number of cells (1×10^6; 5×10^5), which were pre-cultured in monolayer at high or low densities (population H; population L), we have observed a stable and consistent measurement of oxygen by the two systems proving the successful application of the planar imaging sensor for oxygen measurement in cell-seeded BTE scaffolds. Despite the similar characteristics of the oxygen consumption curves, a visible decrease in the actual oxygen concentrations was observed using

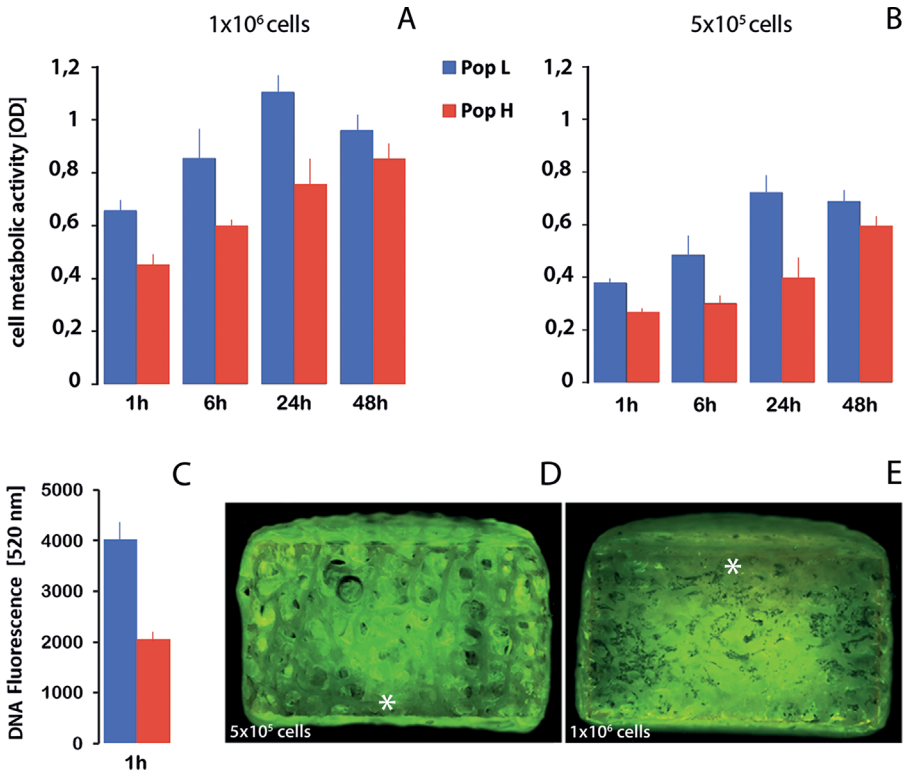

Figure 4. Cell metabolic and proliferation activities of scaffold-seeded hMSCs harvested from low and high confluent populations. (**A**) Metabolic activity of population L and H at 1×10^6 over 48 h. (**B**) Metabolic activity of population L and H at 5×10^5 cells. (**C**) Difference of the DNA content of population L and H one hour after seeding of 1×10^5 cells in a microwell plate. (**D** and **E**) Overview fluorescence images of cell seeded DBM-scaffolds. Micrographs of the Live–Dead staining were captured at the sagittal plane after 24 h (1.25 × objective). Living cells were stained by calcein AM (green) and dead cells by ethidiumbromide-III (red). (**D**) Live–Dead assay of population L at 5×10^5 cells and (**E**) at 1×10^6 cells (Bottom side is marked by an asterisk "*"). (n = 3 ± SD; OD = Optical Density; Scaffold wide = 9 mm).

the imaging system compared to the needle-type control (Fig. 3). This average 3.3% difference in values, obtained by the two oxygen measurement systems may have several reasons. In contrast to the classical needle type sensor, measuring only one spot, the planar optical sensor measures a 2D area. Each pixel of an oxygen map is one oxygen value. As previously demonstrated, oxygen gradients arise around both type of sensors at the bottom as well as in the center of the in vitro cultured 3D scaffold because of limited diffusion capacity (Carrier et al., 2002; Volkmer et al., 2008). The more pronounced oxygen consumption recorded by the oxygen-imaging sensor is a consequence of the different measuring locations. Due to the static seeding process, at the outer surfaces of the DBM-scaffold, where the oxygen imaging sensor measures, cell density is higher than in the center, where the control sensor is localized (Wendt et al., 2003). Consequently, the higher cell number leads to greater cell metabolism resulting in higher oxygen consumption (Santoro et al., 2011; Yamada et al., 1990). A further explanation could be the distinct properties of the needle-type control sensor. This local measuring is prone for errors because it delivers only randomized and not averaged data over an area. Furthermore, the penetration with the needle causes damage to the scaffold material, so that fresh medium can reach the center of the DBM-scaffold, supplying it potentially with additional oxygen.

Characterization of Cell-Seeding Strategies by Application of the Planar Oxygen-Imaging Sensor

In the present study, we have utilized the novel oxygen imaging sensor to evaluate the effect of monolayer plating density of pre-cultured hMSCs on oxygen consumption of cell-loaded, three-dimensional bone tissue engineering constructs. Currently, there are no defined standards for monolayer expansion, harvesting, and seeding of hMSCs into 3D scaffolds (Colter et al., 2000; Neuhuber et al., 2008; Polzer et al., 2014). Among the many factors which can affect the properties of in vitro cultured 3D constructs, such as cell type, scaffold material, pore size, and functionalization, the cell density at the time of harvest may have pivotal role in the modulation of cell proliferation and the final tissue quality. In monolayer culture, high cell density with existing cell–cell contacts usually results in cell cycle arrest and an early termination of cell proliferation due to the down-regulation of cell proliferation genes (Balint et al., 2015; Ho et al., 2011; Kim et al., 2014; Shay and Wright, 2000). In contrast, low cell density leads to an up-regulation of these genes and increased proliferation rate (Kim et al., 2014).

Oxygen consumption of in vitro cultured 2D-3D constructs depends primarily on cell metabolic activity and proliferation (Guarino et al.,

2004; Janssen et al., 2006; Santoro et al., 2011; Yamada et al., 1990). An increase in the number of cells leads to a decrease of the oxygen concentration (Santoro et al., 2011; Yamada et al., 1990) and its continuing decline causes apoptosis or necrosis (Volkmer et al., 2008, 2010). In our study, hMSCs were harvested at low confluence (30–40%, population L) or high confluence (70–80%, population H) and seeded at two different densities (0.5 and 1 million cells) into DBM scaffolds, followed by the measurement of the oxygen consumption for 24 h. Our results show a highly significant difference in oxygen consumption between the two populations (Fig. 3). Cells harvested at low confluence displayed fast exponential decrease of oxygen to 5% within 4 h and reached 0% after 8–10 h (e.g., 1 million cells, Fig. 3B). In contrast, cells harvested at higher confluence exhibited very slow and rather linear than exponential oxygen consumption over the 24 h period without reaching the zero line (Fig. 3A). To our knowledge this difference of oxygen consumption of bone grafts seeded with population L and H has not been shown previously. In population L, the oxygen concentration was three times lower after 4 h and five times lower after 5 h compared with population H (e.g., 1 million cells). Our oxygen results indicate the well-known fact that MSCs with low confluence of 30–40% at the time of harvest (population L) own a much stronger growth potential in comparison to cells with higher confluence of 70–80% (population H). Furthermore, our data indicate that not only the seeding density on a scaffold but also the cell confluence on culture dishes at the time point of harvest is of major importance for BTE (Fig. 3). When harvested at low confluency, cells are in a very potent growth phase. If harvested at high confluency, a lot of cells have already reached steady state and their metabolic and growth activity is decreased. This fact is also evident in the oxygen demand (Fig. 3) and in the metabolic and growth activities (Fig. 4).

The result goes in line with previous studies showing several disadvantages of long expansion and in vitro 3D cultivation time. Besides the arising hypoxia in 3D-scaffolds, replicative senescence of hMSC occurs (Kassem et al., 1997), which impairs both proliferation and differentiation potential (Balint et al., 2015; Geissler et al., 2012; Stenderup et al., 2003). During in vitro expansion with a typical confluence of 70–80%, osteogenic differentiation potential decreases and there is an age-related shift from osteogenic to adipogenic differentiation (Balint et al., 2015; Geissler et al., 2012; Kim et al., 2012). Furthermore, the risk of malignant transformation of cells in long-term cultures due to chromosomal rearrangement, gene mutation, and epigenetic changes has been reported (Rosland et al., 2009). Consequently, a short-run and effective seeding procedure of MSC is advised for BTE purposes (Balint et al., 2015; Xing et al., 2011).

In addition, cell metabolic activity results (Fig. 4A and B) also indicated that a short culture time of less than 24 h is favorable, especially when using the potent population L. It has been shown, that the time point of harvest plays an important role in cell metabolism and proliferation potential in scaffold cultures. The metabolic and proliferation activity of population L was always 30–50% higher than in population H (Fig. 4A–C). Our data shows an increase of metabolic activity over 24 h. However, metabolic activity of population L decreased after 24 h, whereas population H still keeps growing. These observations together with the oxygen data support the suggestion that culture time of potent mesenchymal stem cells in the early log phase should be as short as possible in a static, in vitro 3D tissue culture.

It can be concluded, that increased oxygen consumption is one of the first symptoms of an imminent metabolic crisis in a scaffold culture. Therefore, measurement of oxygen concentration is an appropriate warning tool for early detection of hypoxia-induced oxidative stress, metabolic reprogramming, and imminent cell death.

Taken together, here we introduced a novel way of oxygen measurement for cell-seeded scaffolds used in BTE by the application of a foil-type, 2D-oxygen imaging sensor. The application of the sensor allowed analysis of different cell seeding strategies of scaffolds by monitoring the oxygen consumption at the critical lower surface. We noticed that the amount of hMSCs loaded on scaffolds can be verifiable increased by harvesting at low, 30–40% of cell density before scaffold seeding. In addition, because of a recognizable and traceable spurt of growth in the log phase at low confluence at harvest, an early transplantation of the MSC-scaffold construct after a seeding time of only 4 until 8 h, for a density of 1×10^6 cells, is feasible. If longer culture time is required, the 2D-sensor could be combined with a perfusion system to prevent harmful hypoxia.

The oxygen-imaging sensor could be also applied for further optimizations of BTE constructs. It is conceivable to use the sensor, for example, to pre-select scaffold materials, to choose the ideal pore size, for the optimization of cell functionality by scaffold coatings or for the characterization of co-culture combination. Additionally, the vascularisation of artificial bone grafts by co-culturing of endothelial cells should be of great interest in BTE (Nguyen et al., 2012). The development of in vitro angiogenesis inside a scaffold could be potentially monitored using the oxygen-imaging sensor by detecting changes in oxygen tension associated with vessel-like tube formations.

The new method of oxygen measurement introduced here can be used for different 3D culture systems, such as hydrogels, solid scaffolds, tissue-bioreactors, and microfluidic systems. The sensor foil can be easily adapted to the culture system, for example at critical feeding areas, such as the interface between scaffold and culture vessel. The sensor is non-invasive, flexible, and reusable and enables online monitoring and mapping of oxygen. In combination with a feedback system it can be used to control the nutrient supply in BTE systems.

The authors are grateful to Professor Jürgen Plitzko from the MPI of Biochemistry for helpful comments. This project was partly funded by the Bayerische Forschungsstiftung.

References

Ahlmann E, Patzakis M, Roidis N, Shepherd L, Holtom P. 2002. Comparison of anterior and posterior iliac crest bone grafts in terms of harvest-site morbidity and functional outcomes. J Bone Joint Surg Am 84-A(5):716–720.

Balint R, Richardson SM, Cartmell SH. 2015. Low-density subculture: A technical note on the importance of avoiding cell-to-cell contact during mesenchymal stromal cell expansion. J Tissue Eng Regen Med 9(10):1200–1203.

Benjamin S, Sheyn D, Ben-David S, Oh A, Kallai I, Li N, Gazit D, Gazit Z. 2013. Oxygenated environment enhances both stem cell survival and osteogenic differentiation. Tissue Eng Part A 19(5-6):748–758.

Bocker W, Yin Z, Drosse I, Haasters F, Rossmann O, Wierer M, Popov C, Locher M, Mutschler W, Docheva D. 2008. Introducing a single-cell-derived human mesenchymal stem cell line expressing hTERT after lentiviral gene transfer. J Cell Mol Med 12(4):1347–1359.

Carrier RL, Rupnick M, Langer R, Schoen FJ, Freed LE, Vunjak-Novakovic G. 2002. Perfusion improves tissue architecture of engineered cardiac muscle. Tissue Eng 8(2):175–188.

Ceccarelli G, Bloise N, Vercellino M, Battaglia R, Morgante L, De Angelis MG, Imbriani M, Visai L. 2013. In vitro osteogenesis of human stem cells by using a three-dimensional perfusion bioreactor culture system: A review. Recent Pat Drug Deliv Formul 7(1):29–38.

Colter DC, Class R, DiGirolamo CM, Prockop DJ. 2000. Rapid expansion of recycling stem cells in cultures of plastic-adherent cells from human bone marrow. Proc Natl Acad Sci U S A 97(7):3213–3218.

Dimitriou R, Jones E, McGonagle D, Giannoudis PV. 2011. Bone regeneration: Current concepts and future directions. BMC Med 9:66.

Elsalanty ME, Genecov DG. 2009. Bone grafts in craniofacial surgery. Craniomaxillofac Trauma Reconstr 2(3):125–134.

Fayaz HC, Giannoudis PV, Vrahas MS, Smith RM, Moran C, Pape HC, Krettek C, Jupiter JB. 2011. The role of stem cells in fracture healing and nonunion. Int Orthop 35(11):1587–1597.

Geissler S, Textor M, Kuhnisch J, Konnig D, Klein O, Ode A, Pfitzner T, Adjaye J, Kasper G, Duda GN. 2012. Functional comparison of chronological and in vitro aging: Differential role of the cytoskeleton and mitochondria in mesenchymal stromal cells. PLoS ONE 7(12):e52700.

Guarino RD, Dike LE, Haq TA, Rowley JA, Pitner JB, Timmins MR. 2004. Method for determining oxygen consumption rates of static cultures from microplate measurements of pericellular dissolved oxygen concentration. Biotechnol Bioeng 86(7):775–787.

Hernlund E, Svedbom A, Ivergard M, Compston J, Cooper C, Stenmark J, McCloskey EV, Jonsson B, Kanis JA. 2013. Osteoporosis in the European Union: Medical management, epidemiology and economic burden. A report prepared in collaboration with the International Osteoporosis Foundation (IOF) and the European Federation of Pharmaceutical Industry Associations (EFPIA). Arch Osteoporos 8(1–2):136.

Ho JH, Chen YF, Ma WH, Tseng TC, Chen MH, Lee OK. 2011. Cell contact accelerates replicative senescence of human mesenchymal stem cells independent of telomere shortening and p53 activation: Roles of Ras and oxidative stress. Cell Transplant 20(8):1209–1220.

Hofmann J, Meier RJ, Mahnke A, Schatz V, Brackmann F, Trollmann R, Bogdan C, Liebsch G, Wang X, Wolfbeis OS. 2013. Ratiometric luminescence 2D in vivo imaging and monitoring of mouse skin oxygenation. Methods Appl Fluoresc 1(4):045002.

Janssen FW, Hofland I, van Oorschot A, Oostra J, Peters H, van Blitterswijk CA. 2006. Online measurement of oxygen consumption by goat bone marrow stromal cells in a combined cell-seeding and proliferation perfusion bioreactor. J Biomed Mater Res A 79(2):338–348.

Janssen FW, van Dijkhuizen-Radersma R, Van Oorschot A, Oostra J, de Bruijn JD, Van Blitterswijk CA. 2010. Human tissue-engineered bone produced in clinically relevant amounts using a semi-automated perfusion bioreactor system: A preliminary study. J Tissue Eng Regen Med 4(1):12–24.

Kassem M, Ankersen L, Eriksen EF, Clark BF, Rattan SI. 1997. Demonstration of cellular aging and senescence in serially passaged long-term cultures of human trabecular osteoblasts. Osteoporos Int 7(6):514–524.

Kim DS, Lee MW, Yoo KH, Lee TH, Kim HJ, Jang IK, Chun YH, Kim HJ, Park SJ, Lee SH. 2014. Gene expression profiles of human adipose tissue-derived mesenchymal stem cells are modified by cell culture density. PLoS ONE 9(1):e83363.

Kim M, Kim C, Choi YS, Kim M, Park C, Suh Y. 2012. Age-related alterations in mesenchymal stem cells related to shift in differentiation from osteogenic to adipogenic potential: Implication to age-associated bone diseases and defects. Mech Ageing Dev 133(5):215–225.

Korompilias AV, Beris AE, Lykissas MG, Kostas-Agnantis IP, Soucacos PN. 2011. Femoral head osteonecrosis: Why choose free vascularized fibula grafting. Microsurgery 31(3):223–228.

Malladi P, Xu Y, Chiou M, Giaccia AJ, Longaker MT. 2006. Effect of reduced oxygen tension on chondrogenesis and osteogenesis in adipose-derived mesenchymal cells. Am J Physiol Cell Physiol 290(4):C1139–C1146.

Meier JK, Prantl L, Muller S, Moralis A, Liebsch G, Gosau M. 2012. Simple, fast and reliable perfusion monitoring of microvascular flaps. Clin Hemorheol Microcirc 50(1–2):13–24.

Neuhuber B, Swanger SA, Howard L, Mackay A, Fischer I. 2008. Effects of plating density and culture time on bone marrow stromal cell characteristics. Exp Hematol 36(9):1176–1185.

Nguyen LH, Annabi N, Nikkhah M, Bae H, Binan L, Park S, Kang Y, Yang Y, Khademhosseini A. 2012. Vascularized bone tissue engineering: Approaches for potential improvement. Tissue Eng Part B Rev 18(5):363–382.

Ochs CJ, Kasuya J, Pavesi A, Kamm RD. 2014. Oxygen levels in thermoplastic microfluidic devices during cell culture. Lab Chip 14(3):459–462.

Oryan A, Alidadi S, Moshiri A, Maffulli N. 2014. Bone regenerative medicine: Classic options, novel strategies, and future directions. J Orthop Surg Res 9(1):18.

Pederson WC, Person DW. 2007. Long bone reconstruction with vascularized bone grafts. Orthop Clin North Am 38(1):23––35.

Polzer H, Volkmer E, Saller MM, Prall WC, Haasters F, Drosse I, Wilhelmi A, Mutschler W, Schieker M. 2014. Comparison of different strategies for in vivo seeding of prevascularized scaffolds. Tissue Eng Part C Methods 20(1):11–18.

Radisic M, Malda J, Epping E, Geng W, Langer R, Vunjak-Novakovic G. 2006. Oxygen gradients correlate with cell density and cell viability in engineered cardiac tissue. Biotechnol Bioeng 93(2):332–343.

Rosland GV, Svendsen A, Torsvik A, Sobala E, McCormack E, Immervoll H, Mysliwietz J, Tonn JC, Goldbrunner R, Lonning PE. 2009. Long-term cultures of bone marrow-derived human mesenchymal stem cells frequently undergo spontaneous malignant transformation. Cancer Res 69(13):5331–5339.

Santoro R, Krause C, Martin I, Wendt D. 2011. On-line monitoring of oxygen as a non-destructive method to quantify cells in engineered 3D tissue constructs. J Tissue Eng Regen Med 6(9):696–701.

Shay JW, Wright WE. 2000. Hayflick, his limit, and cellular ageing. Nat Rev Mol Cell Biol 1(1):72–76.

Stenderup K, Justesen J, Clausen C, Kassem M. 2003. Aging is associated with decreased maximal life span and accelerated senescence of bone marrow stromal cells. Bone 33(6):919–926.

Tschiersch H, Liebsch G, Borisjuk L, Stangelmayer A, Rolletschek H. 2012. An imaging method for oxygen distribution, respiration and photosynthesis at a microscopic level of resolution. New Phytol 196(3):926–936.

Tschiersch H, Liebsch G, Stangelmayer A, Borisjuk L, Rolletschek H. 2011. Planar oxygen sensors for non invasive imaging in experimental biology. In: Minin I, editor. Microsensors. Rijeka, Croatia: InTech. p 281–294.

Volkmer E, Drosse I, Otto S, Stangelmayer A, Stengele M, Kallukalam BC, Mutschler W, Schieker M. 2008. Hypoxia in static and dynamic 3D culture systems for tissue engineering of bone. Tissue Eng Part A 14(8):1331–1340.

Volkmer E, Kallukalam BC, Maertz J, Otto S, Drosse I, Polzer H, Bocker W, Stengele M, Docheva D, Mutschler W. 2010. Hypoxic preconditioning of human mesenchymal stem cells overcomes hypoxia-induced inhibition of osteogenic differentiation. Tissue Eng Part A 16(1):153–164.

Volkmer E, Otto S, Polzer H, Saller M, Trappendreher D, Zagar D, Hamisch S, Ziegler G, Wilhelmi A, Mutschler W. 2012. Overcoming hypoxia in 3D culture systems for tissue engineering of bone in vitro using an automated, oxygen-triggered feedback loop. J Mater Sci Mater Med 23(11):2793–2801.

Wendt D, Marsano A, Jakob M, Heberer M, Martin I. 2003. Oscillating perfusion of cell suspensions through three-dimensional scaffolds enhances cell seeding efficiency and uniformity. Biotechnol Bioeng 84(2):205–214.

Woertgen C, Warnat J, Brawanski A, Liebsch G. 2009. Non-invasive measurement of the superficial cortical oxygen partial pressure. Adv Exp Med Biol 645:167–173.

Xing Z, Xue Y, Danmark S, Finne-Wistrand A, Arvidson K, Hellem S, Yang ZQ, Mustafa K. 2011. Comparison of short-run cell seeding methods for poly(L-lactide-co-1,5-dioxepan-2-one) scaffold intended for bone tissue engineering. Int J Artif Organs 34(5):432–441.

Yamada K, Furushou S, Sugahara T, Shirahata S, Murakami H. 1990. Relationship between oxygen-consumption rate and cellular-activity of mammalian-cells cultured in serum-Free media. Biotechnology and Bioengineering 36(7):759–762.

Yeatts AB, Choquette DT, Fisher JP. 2013. Bioreactors to influence stem cell fate: Augmentation of mesenchymal stem cell signaling pathways via dynamic culture systems. Biochim Biophys Acta 1830(2):2470–2480.